

Effect of Variation of Angle of Attack on Lift and Drag Coefficient of Flat Plate Wing on Flying Inflatable Boat

Nafroni¹, Byan Wahyu Riyandwita², Palka Adripta³
{byan.wr@universitaspertamina.ac.id²}

Department of Mechanical Engineering, Faculty of Industrial Technology, Universitas Pertamina, Indonesia^{1,2}

Department of Technical (Engineering, Construction & Facilities Maintenance), Elnusa Petrofin, Indonesia³

Abstract: The use of Flying Inflatable Boat (FIB) vehicles has caught the attention in applications like search and rescue operations, military surveillance, and recreational activities. The aerodynamics of flat wings of FIB needs to investigate so that the performance, safety and efficiency vehicles can be improved. Changes in angle of attack, velocity, and air density affect lift and drag coefficients are evaluated using Computational Fluid Dynamics (CFD) analysis. Results show that the lift coefficient increases until an angle of attack of 34° meanwhile the ratio of C_L/C_D is increased up to angle of 5° . However, as the angle of attack (AOA) continues to increase the drag coefficient also rises. It is also found that both the lift coefficient and C_L/C_D ratio increase as the velocity goes up. Additionally, decrease of lift coefficient and C_L/C_D ratio accompanied by an increase in drag coefficient is observed as air density decreases.

Keywords: Flying Inflatable Boat, Flat wing, Angle of attack, Lift coefficient, C_L/C_D ratio

1 Introduction

Flying inflatable boat (FIB) is one of the flying boat vehicles that is quite popular as an air vehicle in several countries. The first to leave water flying boat (Le Canard) was invented by Henri Fabre in 28 March 1910 [1]. FIB is a combination of an inflatable boat with a hanging kite wing. In Indonesia, FIB is still few in existence, it can even be said that it is only owned personally by a few people. FIB with wheel type can run on the sea or on land. In general, this FIB is driven by a pilot carrying one passenger. To fly FIB requires a lift force that is greater than the force of gravity. For that we need an optimal wing design and in accordance with FIB conditions. FIB can be categorized as microlight amphibian vehicles since its maximum take off weight (MTOW) is less than 450 kg when flown solo or maximum of 650 kg with two persons with minimum speed at MTOW less than 83 km/h (51.67 mph) based on sporting code of Fédération Aéronautique Internationale (FAI) [2]. In Indonesia, there are still few people who are interested in FIB vehicles, so it can be a new opportunity to develop this vehicle. This FIB can be used to develop tourism and boost the economy in Indonesia.

Accidents on FIB flights can occur, especially when they are exposed to wind gusts and turbulence due to their lightweight nature. To minimize or avoid accidents it is important to understand the characteristics of the wings used. Since FIB flight is controlled manually by the pilot, this knowledge enables management of FIB flights, including setting the angle of attack and maintaining a suitable FIB speed. These factors are closely linked to the drag, lift and thrust forces exerted by the wings, which can be estimated accordingly. To determine the magnitude of the coefficient of lift and drag wings can be tested in a wind tunnel (wind tunnel). However, the costs required are not small and the testing time also takes a some times. Therefore, the use of Computational Fluid Dynamics (CFD) greatly helps reduce the cost and time in estimating the lift and drag coefficients.

In this study, a swept back flat plate wing design of an airfoil shaped wing is selected because it is easier to manufacture. Swept wings are longer than straight wings, which helps reduce turbulence by slowing down the friction of air as it moves across the wing surface. Although cambered plates offer better characteristics and performance at higher Reynolds numbers (60,000 to 200,000) they also contribute to a higher drag coefficient [3]. Since the actual flight of FIB will have a cambered shape when using flexible material for the wing and exhibit similar aerodynamics trends as the flat plate wing, the flat plate wing is used to analyze in order to simplify the simulation.

The stability of the wake profile and the force experienced by the body at low Reynolds numbers were found to be influenced by the aspect ratio and angle of attack [4]. The formation and subsequent separation of leading edge vortices, which eventually turned into hairpin vortices after an initial impulsive movement were observed when it comes to low aspect ratio of rectangular plates. This phenomenon is quite similar, to dynamic stall observed behind pitching plates. Although the aspect ratio has been identified as the parameter affecting aerodynamic characteristics such as lift, drag and pitching moment at low Reynolds numbers, around 10^5 [5], the aspect ratio is not yet considered in this study since the Reynolds numbers are in the range of 5×10^5 to 1.9×10^6 and it will investigated in the future.

This study aims to analyze the lift coefficient, drag coefficient, pressure distribution, and velocity distribution on the flat plate flying inflatable boat wing design with various simulation parameters such as angle of attack, FIB speed, and air density (representing FIB flight altitude).

2 METHODOLOGY

2.1 Simulation

The wing design will be analyzed through CFD simulation using the Ansys 2019 R3 software. In this simulation, the flow is turbulent because the Reynold number is around 10^6 , and for a flat surface, the critical Reynolds number is approximately 5×10^5 [6]. The k omega SST was selected as the turbulence model because it has gained popularity in simulations of flow, around bluff bodies. This choice is based on its reputation, for being efficient and accurate [7, 8]. The k-epsilon model is useful in predicting the flow from the wall when dealing with high Reynolds numbers. On the hand when it comes to flow around the wall at low Reynolds numbers the k-omega model proves to be more effective. Therefore simulations on flow around wing walls in this study use the k-omega model as it has advantages over k-epsilon model.

Because the wings are symmetrical and to speed up the simulation, the simulation is only done on half the wings. The simulation conditions used in can be seen in **Table 1**. Variations in

density, viscosity, temperature, and air pressure are determined based on altitudes of 0 ft (0 m), 5,000 ft (1,524 m), and 10,000 ft (3,048 m). While the FIB speed variation or velocity inlet for the wing uses multiples of 20 mph until the maximum speed of the FIB engine is 55 mph. speed variations are 15 mph (6.7 m/s), 35 mph (15.64 m/s), and 55 mph (24.58 m/s) since it was mentioned previously that minimum speed at MTOW is less than 83 km/h (51.57 mph) based on sporting code of Fédération Aéronautique Internationale (FAI) [2]. To enhance the simulations speed it is decided to adjust the Angle of Attack (AOA) in increments of 5°, from 0, to 45°. This is because stalls tend to occur when the AOA reaches a point, which typically falls within the range of 16 to 20° [9]. When starting to approach the stall angle, use the angle of attack in multiples of 1°.

Table 1. Simulation conditions.

Parameter	Value
Solver	3D, <i>Pressure based, Time: steady, Unchecked gravity</i>
Model Viscous	SST k-Omega
Material	<i>Fluid – Air</i>
Inlet boundary condition	<i>Velocity inlet</i>
Wing boundary condition	<i>Wall</i>
Symetry boundary condition	<i>Symmetry</i>
Wall boundary condition	<i>Wall</i>
Outlet boundary condition	<i>Pressure outlet</i>
Flow speed (Velocity inlet)	6.7; 15.64; 24.58 (m/s)
Angle of attack (α)	0°, 5°, 10°, 15°, 20°, 25°, 30°, 35°, 40°, 45°

The density values that were varied during the simulation were taken based on data from the U.S. Standard Atmosphere Air Properties at an altitude of 0 ft (0 m) to 10,000 ft (3,048 m) above sea level [10]. The determination of the height of 10,000 ft (3,048 m) above sea level is because additional oxygen supply is needed at that altitude [11]. Variations in air density values based on the altitude can be seen in **Table 2** below.

Table 2. Altitude variation.

Altitude m	Density kg/m^3	Pressure N/m^2	Temp. K	Viscosity $\times 10^{-5} Ns/m^2$
0	1.225	101,325	288	1.789
1,524	1.055	84,309	278	1.741
3,048	0.905	69,692	268	1.692

2.2 Design

The wing type used is the swept back type using assumption of flat plate wing. The span of the wing is 10.3 m with chord root of 2 m and chord tip 1.5 m. The area of the wing is 18.051 m² with sweep angle of 16.23°. The aspect ratio of the wing is 5.8 and taper ratio of 0.75. The details of the swept back wing design used in this study can be seen in **Figure 2**. To reduce the computation requirement, only half of the model is enough to represent the lift and drag coefficients of the wing. The symmetrical wing domain and mesh can be seen in **Figure 3**. Independent mesh study has been performed with mesh number range from 265,628 to

1,531,697 elements. The lift and drag coefficients starts to be constant when the number of mesh is around 831,131 elements, thus this number of mesh is selected to reduce computing time and the minimal computer resources. The cross section of the flat plate wing uses design of flat plate that has 5-to-1 leading & trailing edge elliptical [12]. The thickness of the plate made is 3.81 mm. Details of cross section of the wing can be seen in **Figure 4** below.

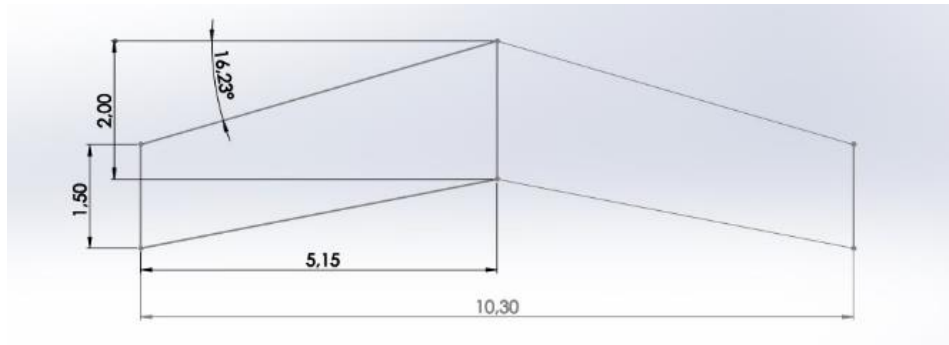


Fig. 2. Swept back symmetrical wing design (in meter).

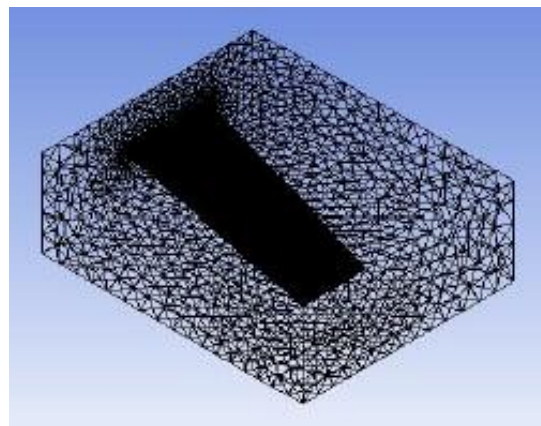


Fig. 3. Swept back symmetrical wing domain and mesh.

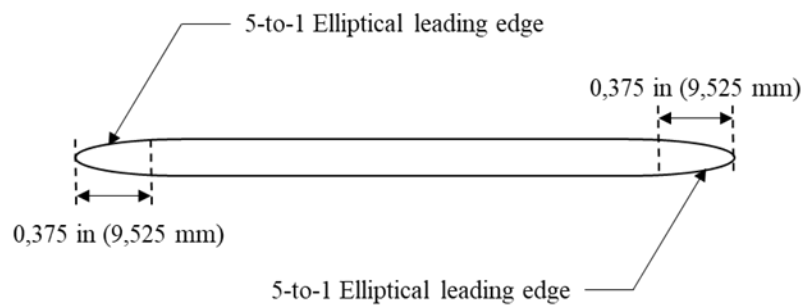


Fig. 4. Flat plate wing cross section.

3 VALIDATION

To validate the simulation, the results are compared with the experiments conducted in previous study. Comparisons were made on flat plate data with the same Reynolds number of 10^5 , taper ratio of 0.75, and aspect ratio of 1 [12]. The only different in this comparison is on the aspect ratio since the swept back flat plate model in this study use an aspect ratio of 5.8. The results of the CFD simulation are almost similar with the experimental values especially below 20° . The average error of this comparison is 7.894% for the lift coefficient and 7.08% for the drag coefficient. Notably the deviation becomes particularly noticeable in the vicinity of the stall angle of attack which corresponds to the maximum lift coefficient. This can be caused by model selection and mesh density especially in the leading and trailing edges. For detail results can be seen in **Figure 5** and **Figure 6**.

The accuracy of simulation results may vary depending on the phenomenon being observed. For instance when comparing fluid dynamics (CFD) simulations, with data from an inductively coupled plasma generator at atmospheric pressure a deviation of approximately 7 – 8% was observed [13]. Similarly when comparing CFD simulations with wind tunnel experiments for openings in a sawtooth building a deviation of around 10% was found [14]. These findings indicate that if the error value is below 10% there is agreement between CFD simulations and experimental results.

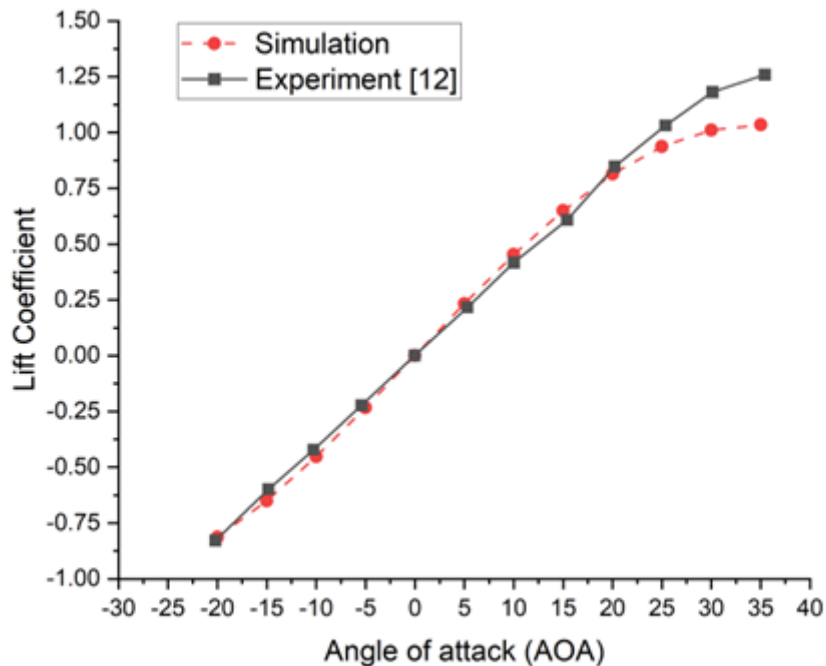


Fig. 5. Comparison of the lift coefficient at different angle of attack between simulation and experiment [12].

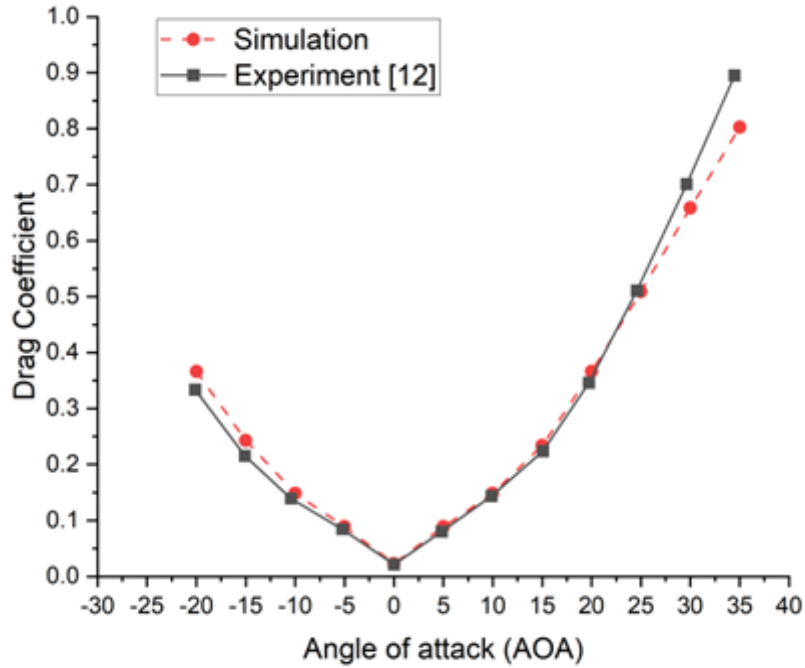


Fig. 6. Comparison of the drag coefficient at different angle of attack between simulation and experiment [12].

4 RESULTS AND DISCUSSION

The swept back type flat plate wing for FIB is simulated using Computational Fluid Dynamics. The parameters observed from the simulation are lift and drag coefficients due to variations in FIB speed, angle of attack, and air density which represent the altitude of FIB.

4.1 Effect of angle of attack

The effect of angle of attack is observed with simulation at height of 3,048 m and speed of 15.64 m/s. **Figure 7** and **Figure 8** shows that the lift coefficient increase as the angle of attack increases to an angle of 34°. After passing through the angle of 34°, the lift coefficient decreases. Meanwhile, the drag coefficient continues to increase as the angle of attack increases. The value of C_L/C_D increases as the angle of attack increases to an angle of 5°. After the angle of 5° the value of C_L/C_D decreased. Previous studies also show that the range of maximum C_L/C_D are between 2 – 5° [15 – 16]. In observing this pressure and velocity contour, the distribution of pressure and velocity that is displayed focuses at the altitude 3,048 m and FIB speed 15.64 m/s. Observations were made on changes in the angle of attack of 10° and 30°.

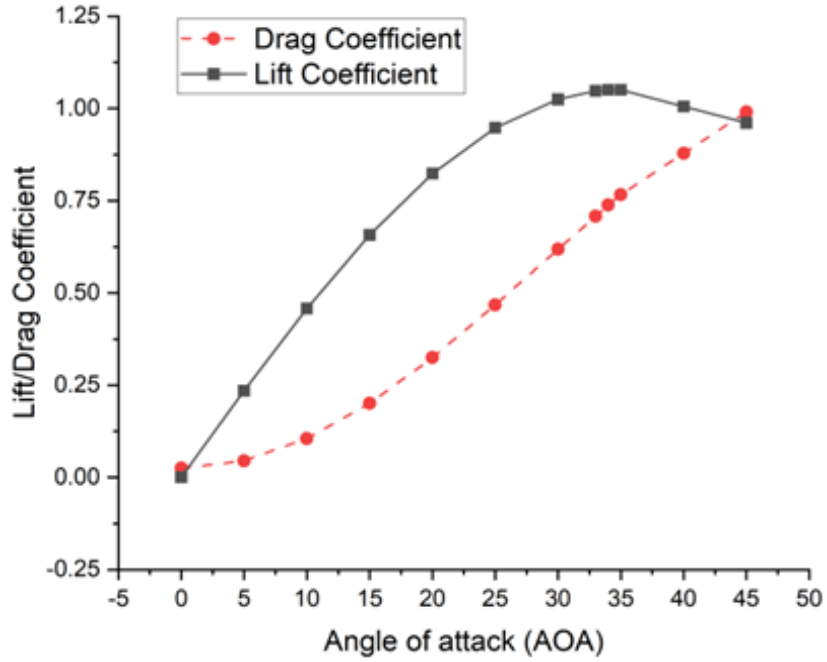


Fig. 7. Coefficient of lift and drag for different angle of attack at altitude of 3,048 m and a FIB speed of 15.64 m/s.

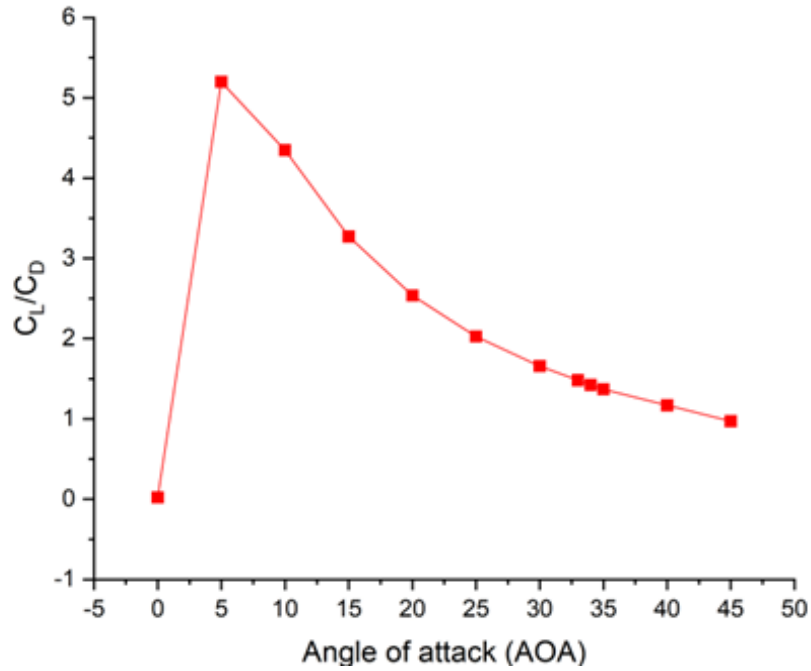


Fig. 8. Lift to drag ratio (C_L/C_D) for different angle of attack at altitude of 3,048 m and a FIB speed of 15.64 m/s.

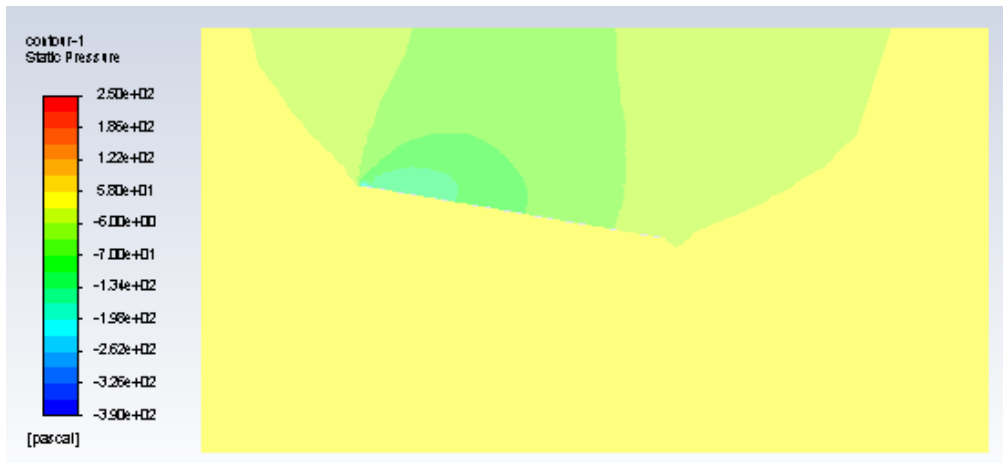


Fig. 9. Pressure contour at angle of attack 10° , altitude of 3,048 m and a FIB speed of 15.64 m/s.

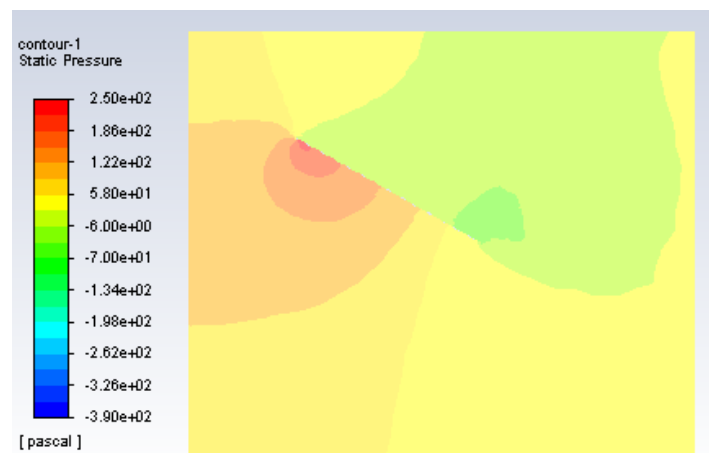


Fig. 10. Pressure contour at angle of attack 30° , altitude of 3,048 m and a FIB speed of 15.64 m/s.

Figure 9 and **Figure 10** shows that the magnitude of the pressure on the undersurface of the wing is greater than the pressure on the top surface of the flat plate flange. This pressure difference causes the lift to be positive, so the wing can be lifted. The maximum pressure is at the lower front end of the flat plate because stagnation occurs at that point, the velocity becomes zero and the molecules at that point create a large pressure. The lowest pressure occurs at the top of the wing surface and the trailing edge of the flat plate. From **Figure 9** and **Figure 10** can be seen that increasing the angle of attack increases the amount of pressure that occurs. The greatest and smallest pressures occurred on the flat plate flange with an angle of attack of 10° are 102.95 Pa and -385.62 Pa. Meanwhile, the largest and smallest pressure occurred on the flat plate wing with an angle of attack of 30° are 244.78 Pa and -250.73 Pa at altitude of 3,048 m and a FIB speed of 15.64 m/s. Changes in the angle of attack cause a change in the location of the Center of Pressure (COP). COP is the point or position where all the aerodynamic forces are

concentrated in the absence of torque. Changes in COP occur because the amount of pressure received by the wing is different. When the angle of attack is greater, the COP will move further towards the leading edge, if the angle of attack is reduced, the COP will move further back towards the trailing edge. COP and CG (center of gravity) are closely related. When the angle of attack increases, the location of the COP will move forward in front of the CG. The load and spread of weight on the wings greatly affect the CG and causes other additional forces that affect the balance of the aircraft.

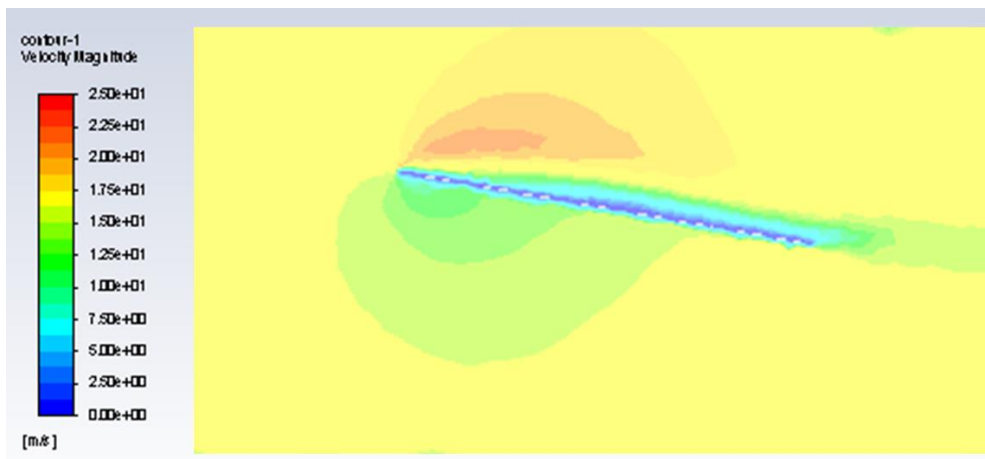


Fig. 11. Velocity contour at angle of attack 10° and 15.64 m/s.

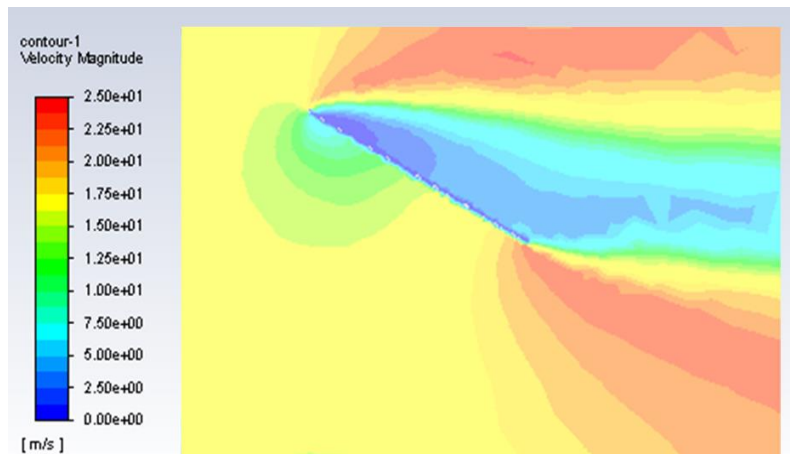


Fig. 12. Velocity contour at angle of attack 30° and 15.64 m/s.

Figure **Figure 11** and **Figure 12** shows the occurrence of air flow separation at the top of the flat plate, where the boundary layer tends to separate from the upper surface of the flat plate. This causes the drag coefficient to increase, while the lift coefficient decreases. This separation condition usually occurs at the stall corner. At an angle variation of 10° the greatest speed is at the front end of the flat plate, while at an angle variation of 30° the greatest speed is at the upper front end and the lower back end of the flat plate surface. The lowest speed is at the top of the

front surface of the flat plate. The greatest speed of the flat plate wing occurs at 23.93 m/s (for an angle of attack of 10°) and 24.10 m/s (for an angle of attack of 30°) at altitude of 3,048 m and a FIB speed of 15.64 m/s.

4.2 Effect of FIB speed

Effect of FIB speed variations is shown with altitude 0 m because it only focuses on observing the changes in FIB speed.

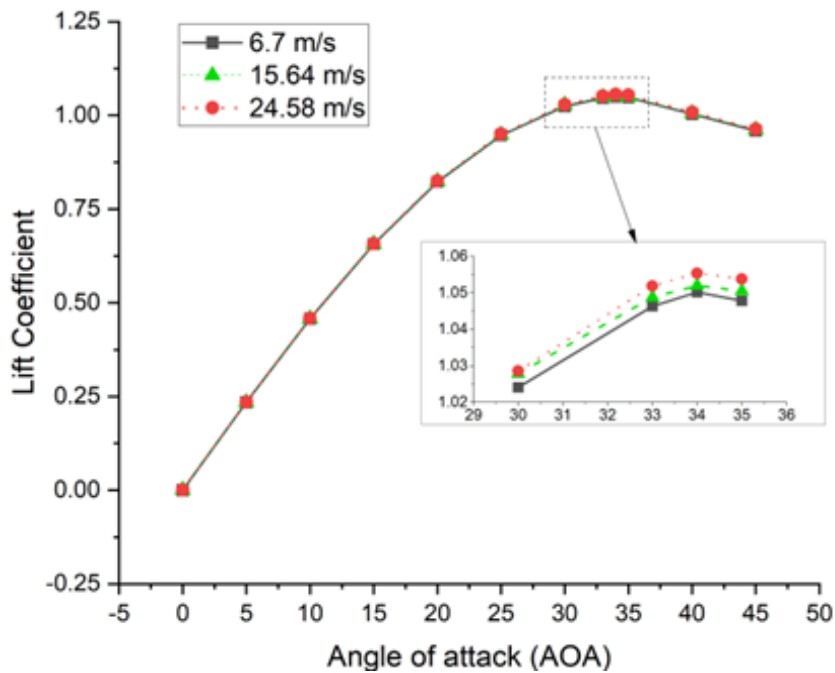


Fig. 13. Lift coefficient for different angle of attack at altitude of 0 m.

Figure 13 shows that the lift coefficient increases with increasing speed from FIB to a certain angle. In the figure the differences in the lift coefficient is very small due to FIB speed variations. Although there are small differences, it can be observed that the lift coefficients increases with the increase of FIB speed. FIB engine thrust determines how much FIB speed is generated. The greater the thrust, the greater the lift coefficient. The effect of the angle of attack on the lift coefficient is directly proportional to a certain angle. The lift coefficient increases as the angle of attack increases to an angle of 34° (the maximum lift coefficient). After passing the 34° angle, the lift coefficient begins to decrease as the angle of attack increases. In this FIB speed variation, the maximum lift coefficient is 1.0554 at speed of 24.58 m/s. Figure 14 shows that the drag coefficient decreases with increasing speed from FIB. The effect of the angle of attack on the lift coefficient is directly proportional. The coefficient of drag increases as the angle increases with steeper trend at high angle of attack. Similar trends has been reported previously for lift coefficient for difference angle of attack for rectangular planforms, $Re = 1 \times 10^5$, with aspect ratio ranged from 0.5 to 2.0 [5].

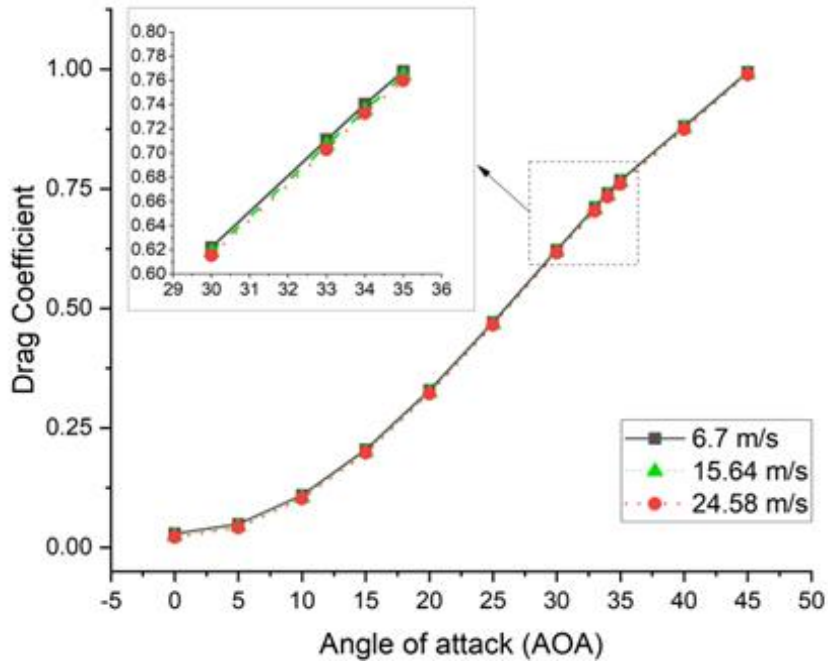


Fig. 14. Drag coefficient for different angle of attack at altitude of 0 m.

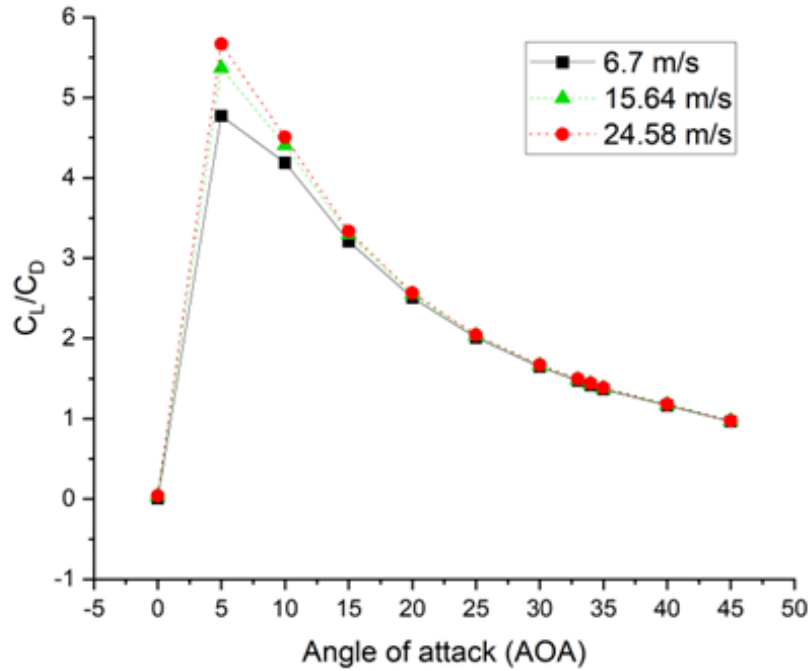


Fig. 15. Graph of the C_L/C_D for different angle of attack at altitude of 0 m.

Figure 15 shows that the ratio of the lift coefficient to the drag coefficient increases with increasing speed from FIB to a certain angle. FIB engine thrust determines how much FIB speed is generated which then affects the lift coefficient and drag coefficient. The greater the thrust, the greater the lift coefficient, while the drag coefficient will be smaller. The influence of the angle of attack on the ratio of C_L/C_D is directly proportional up to the angle of 5° , where the ratio of C_L/C_D increases as the angle of attack increases. After passing the 5° angle, the C_L/C_D ratio decreases. In observing the pressure and velocity contour, the distribution of pressure and velocity that is displayed focuses on the angle of attack 30° and height at 0 m in the following figures. Observations were made on changes in FIB speed of 15.64 m/s and 24.58 m/s.

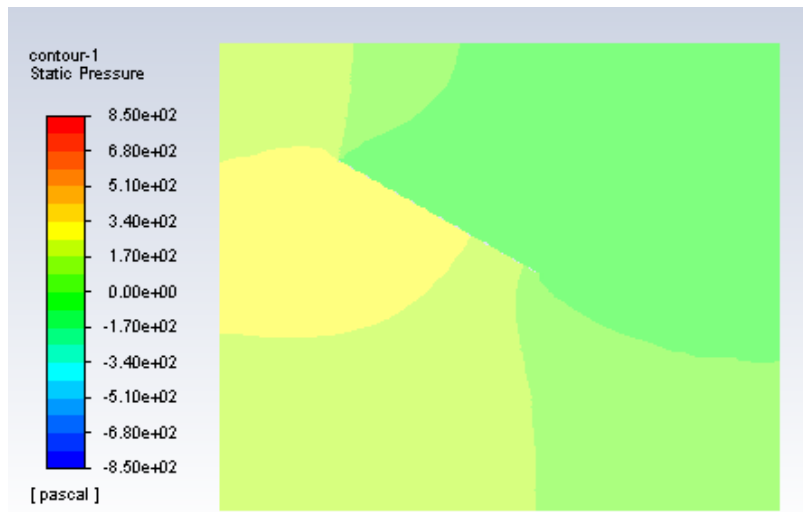


Fig. 16. Pressure contour at FIB speed 15.64 m/s.

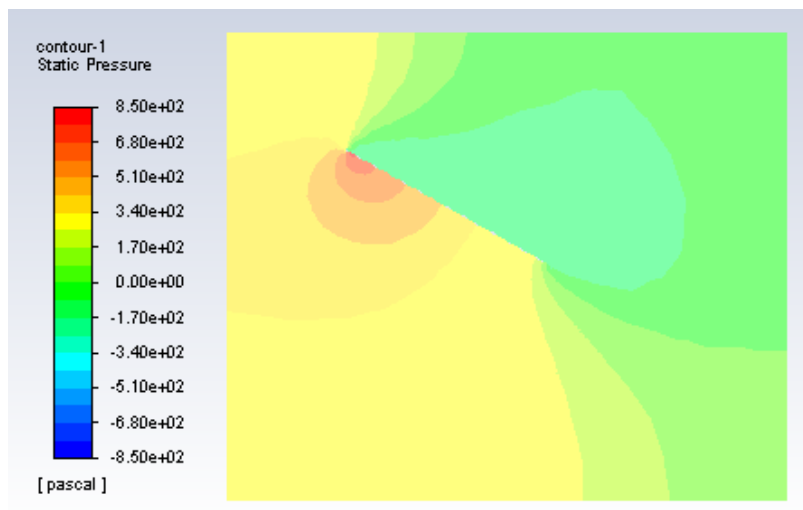


Fig. 17. Pressure contour at FIB speed 24.58 m/s

Figure 16 and **Figure 17** shows that the magnitude of the pressure on the undersurface of the wing is greater than the pressure on the top surface of the flat plate flange. This pressure difference causes the lift to be positive, so the wing can be lifted. The maximum pressure is at the lower front end of the flat plate because stagnation occurs at that point, the velocity becomes zero and at that point create a large pressure. The lowest pressure occurs at the top of the wing surface and the trailing edge of the flat plate. From **Figure 16** and **Figure 17** can be seen that increasing the FIB speed increases the amount of pressure that occurs. The biggest and smallest pressure occurred on the flat plate wing with a speed of 15.64 m/s are 330.995 Pa and -319.844 Pa. Meanwhile, the largest and smallest pressure occurred on the flat plate wing with a speed of 24.58 m/s are 818.22 Pa and -846.045 Pa.

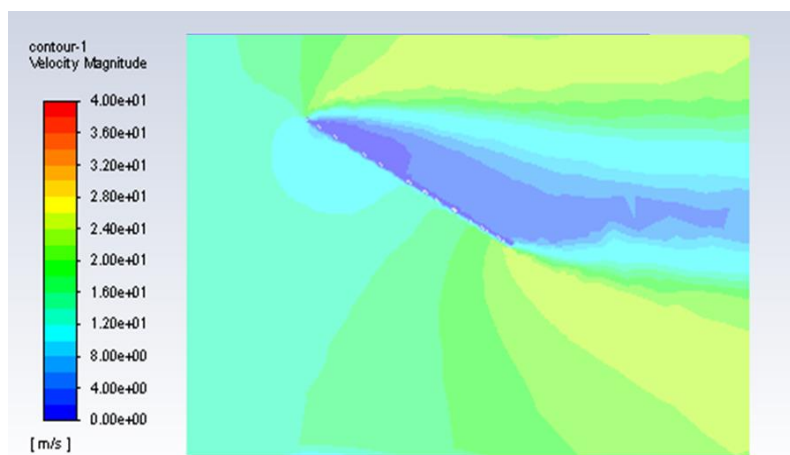


Fig. 18. Velocity contour at FIB speed 15,64 m/s

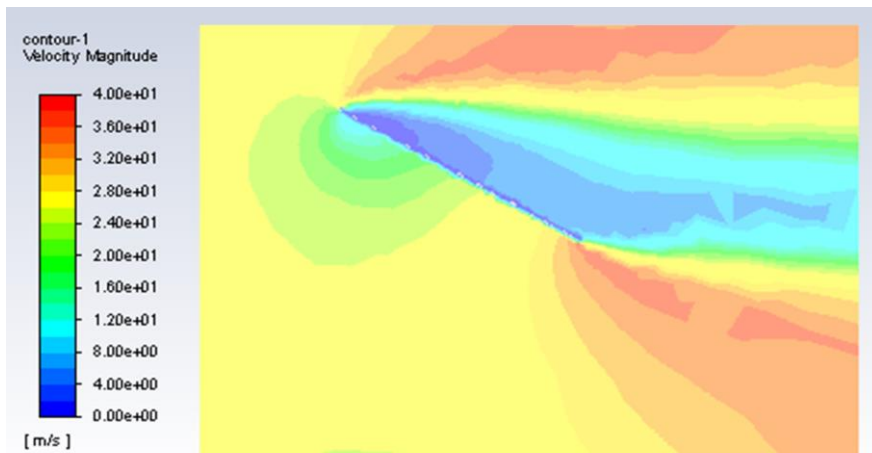


Fig. 19. Velocity contour at FIB speed 24.58 m/s

Figure 18 and **Figure 19** shows the air flow separation at the top of the flat plate, where the boundary layer tends to separate from the surface of the flat plate. This is what causes the drag coefficient to increase, while the lift coefficient decreases when the FIB speed variation

simulation is carried out. The figure shows that the greatest velocity is at the upper front end of the flat plate and the lower back end of the flat plate surface. The lowest velocity is at the top of the front surface of the flat plate. The greatest velocity of the flat plate wing occurs at 24.12 m/s (for a speed of 15.64 m/s) and 37.7 m/s (for a speed of 24.58 m/s).

4.3 Effect of Air density (flying altitude)

In this section the results shown is represented with variations in speed at 6.7 m/s because it only focuses on observing changes in air density (flying altitude). **Figure 20** shows that the lift coefficient decreases as the air density decreases. Variations in values used in the simulation due to differences in altitude are changes in the values of density, dynamic viscosity, temperature, and air pressure. The change in the acceleration of gravity is not used because the simulation is carried out by ignoring the weight of the wing. Meanwhile, **Figure 21** shows that the drag coefficient only slightly increases as air density decreases. Air density affects air pressure. When the air density is getting smaller (the higher the FIB flies) then the air molecule density is getting more tenuous. So that the applied pressure will decrease. This is what causes at a certain height a flying vehicle such as a jet can fly faster than its normal speed. This happens because the air flow at a higher point is more easily penetrated due to the less density of the air. As in the variation of the FIB velocity value, the effect of the angle of attack on the lift coefficient is also directly proportional to an angle of 34° (the maximum lift coefficient). After passing the 34° angle, the lift coefficient begins to decrease as the angle of attack increases. Meanwhile, as in the variation of the FIB velocity value, the effect of the angle of attack on the drag coefficient is also directly proportional. The greater the angle of attack, the greater the drag coefficient.

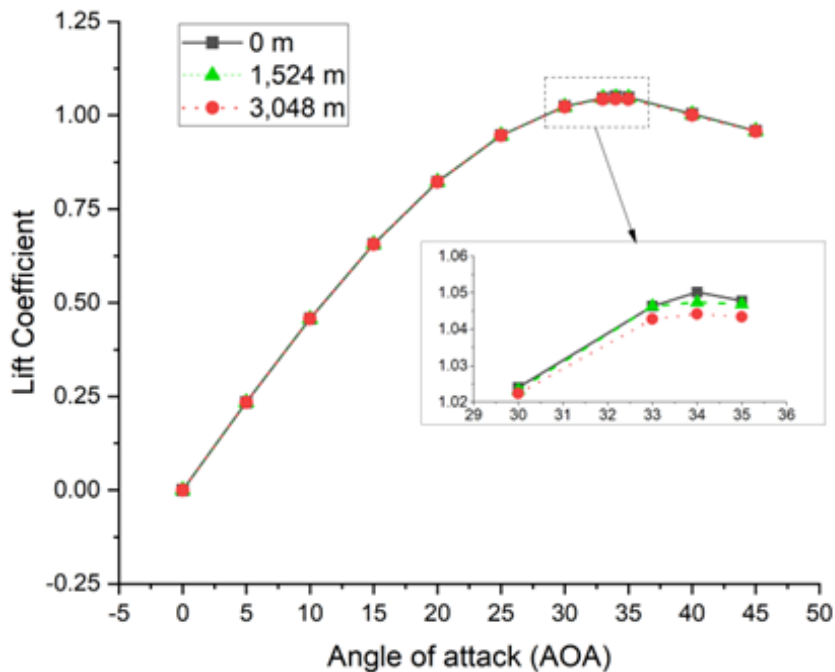


Fig. 20. Lift coefficient for different angle of attack at FIB speed of 6.7 m/s.

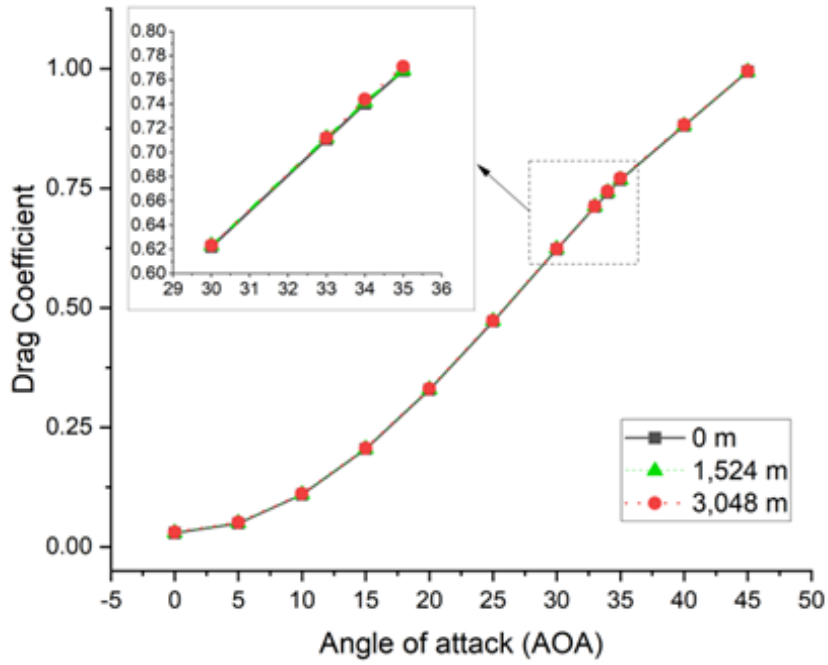


Fig. 21. Drag coefficient for different angle of attack at FIB speed of 6.7 m/s.

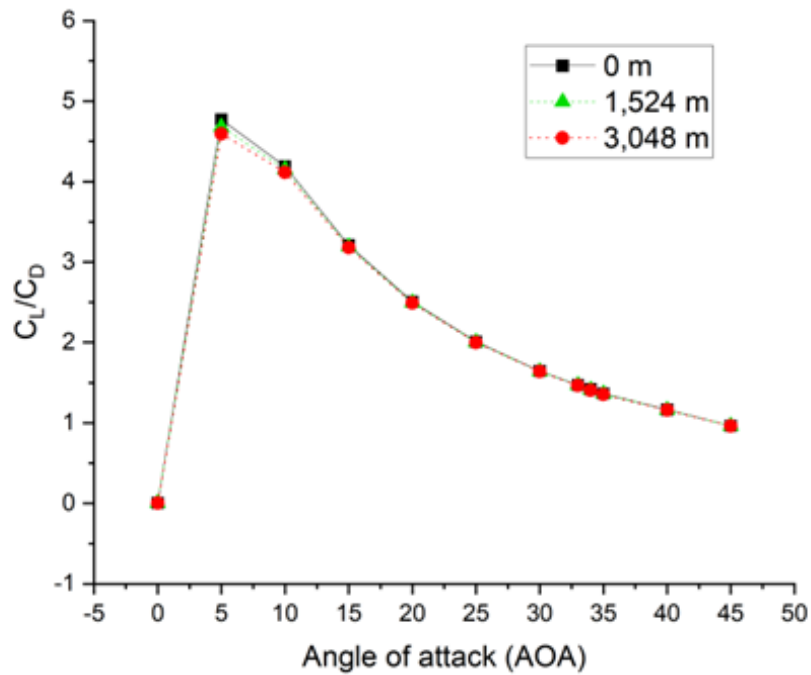


Fig. 22. Graph of the C_L/C_D against the angle of attack at FIB speed of 6.7 m/s.

Figure 22 shows that the ratio of the lift coefficient to the drag coefficient decreases with increasing FIB flying height. This happens because of the decrease in density which causes a decrease in air pressure on the wing walls, so the drag coefficient will slightly increase. The lower the air density, the lower the C_L/C_D ratio. The influence of the angle of attack on the ratio of C_L/C_D is directly proportional to the angle of 5° , where the ratio of C_L/C_D increases as the angle of attack increases. After passing the 5° angle, the C_L/C_D ratio decreases. In observing the pressure and velocity contour, the distribution of pressure and velocity that is displayed focuses on the angle of attack 30° and FIB speed at 15.64 m/s. Observations were made on changes in flying altitude of 0 m and 3048 m.

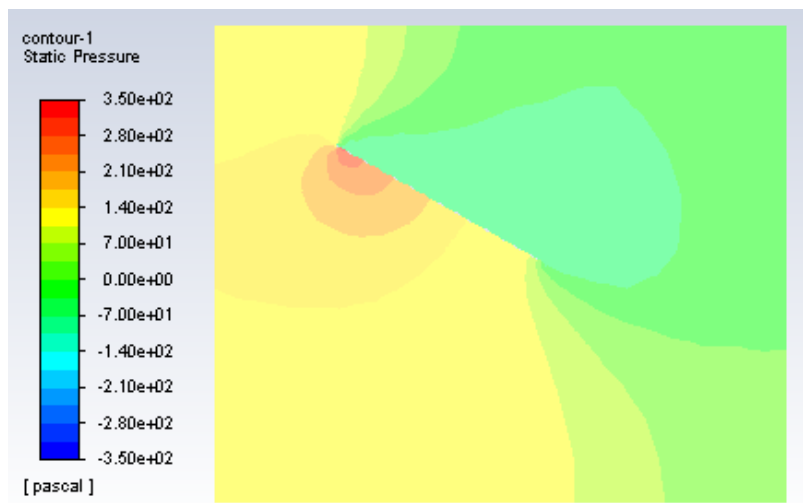


Fig. 23. Pressure contour at altitude 0 m.

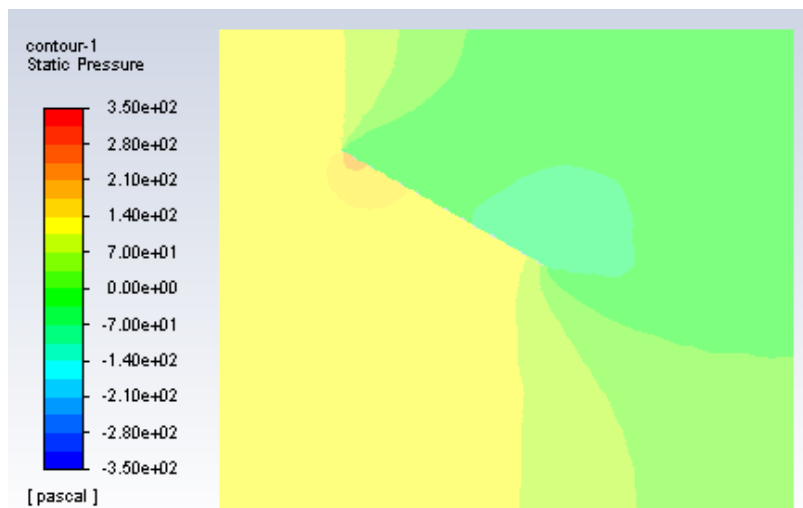


Fig. 24. Pressure contour at altitude 3048 m.

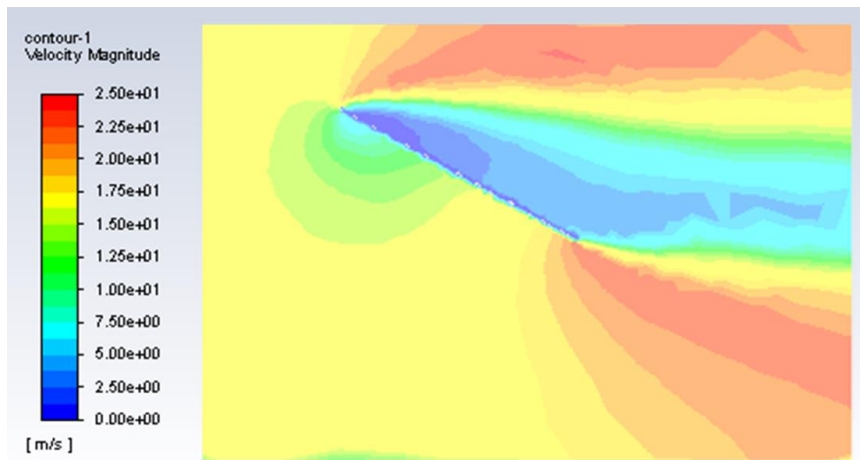


Fig. 25. Velocity contour at altitude 0 m.

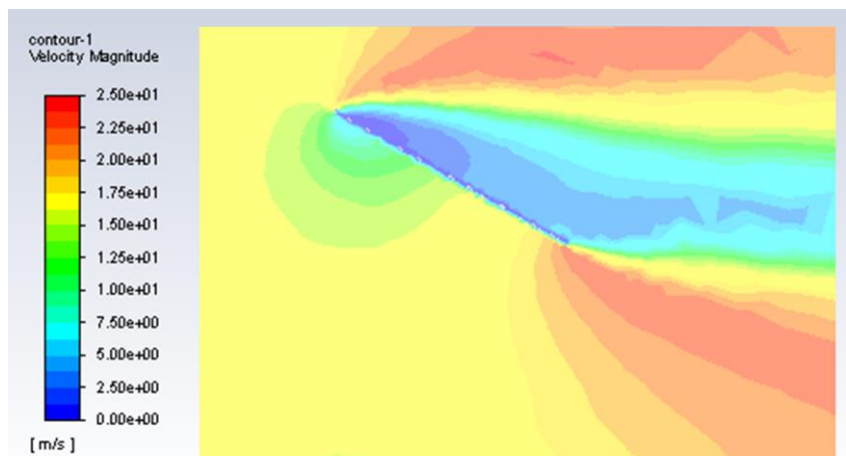


Fig. 26. Velocity contour at altitude 3048 m.

Figure 23 and **Figure 24** shows that the magnitude of the pressure on the undersurface of the wing is greater than the pressure on the top surface of the flat plate flange. This pressure difference causes the lift to be positive, so the wing can be lifted. The maximum pressure is at the lower front end of the flat plate because stagnation occurs at that point, the velocity becomes zero and the molecules at that point create a large pressure. The lowest pressure occurs at the top of the wing surface and the trailing edge of the flat plate. From **Figure 23** and **Figure 24** can be seen that the decrease in air density also reduces the amount of pressure that occurs. The largest and smallest pressures occurred on the flat plate wing with a height of 0 m are 330.99 Pa and -319.84 Pa. Meanwhile, the largest and smallest pressure occurred on the flat plate wing with a height of 3048 m are 244.78 Pa and -250.73 Pa. **Figure 25** and **Figure 26** shows the occurrence of air flow separation at the top of the flat plate, where the boundary layer tends to separate from the surface of the flat plate. This is what causes the drag coefficient to increase, while the lift coefficient to decrease when the density reduction variation simulation is carried out. The figure shows that the greatest velocity is at the upper front end of the flat plate and the

lower back end of the flat plate surface. The lowest velocity is at the top of the front surface of the flat plate. The greatest speed of the flat plate wing occurs at 24.10 m/s (for a height of 3,048 m) and 24.12 m/s (for a height of 0 m).

4.4 Stall speed and cruise speed

Stall speed is the minimum speed required for a Flying inflatable boat (FIB) to be able to produce a lift that is greater than the weight of the FIB. Stall speed occurs when at a certain angle produces the highest lift coefficient. In this study, the lift coefficient has a maximum value at an angle of 34°. Meanwhile, cruise speed is the speed required by FIB to achieve optimal design conditions and economical fuel use. In this condition the speed and altitude are relatively constant. Cruise speed can be calculated using C_L/C_D values. The higher the C_L/C_D , the more aerodynamic the FIB flies. In this study, C_L/C_D has a maximum value when the angle reaches 5°. The FIB weight at takeoff for the simulation is assumed to be the same as the microlight MTOW (Maximal Take Off Weight) of 450 kg. The simulation results at the time of stall speed and cruise speed can be seen in **Table 3** below.

Table 3. Stall & cruise speed

	FIB speed m/s	Lift coefficient	Drag coefficient
Stall (0 m)	19.6	1.0525	0.734
Cruise (1,524 m)	44.7	0.2353	0.0394
Cruise (3,048 m)	48.2	0.2352	0.0396

The stall speed simulation is carried out at a height of 0 m, because the stall speed occurs during the takeoff phase. In this study, FIB that uses flat plate wings has a stall speed of 19.66 m/s (44 mph). This speed is much greater than the FIB made by SEAIR which uses wings with the airfoil concept. The SEAIR-made FIB has a stall speed of 11.17 m/s (25 mph) and the lift is almost 2 times that of a flat plate wing [17]. This proves that the use of an airfoil design on the wing of a flying vehicle is necessary to increase the lift of the flying vehicle. For cruise speed, the flat plate wing is simulated at an altitude of 1,524 m and 3,048 m because the cruise speed occurs when the FIB is already flying. In this simulation, the FIB with flat plate wings has a cruise speed of 44.7 m/s (100 mph) for an altitude of 1,524 m and 48.28 m/s (108 mph) for an altitude of 3,048 m. When compared to the FIB made by SEAIR which has a cruise speed of 20.11 m/s (45 mph) [17], it can be said that the wing with the airfoil concept is much more aerodynamic than the flat plate wing. Looking at the flight characteristics of the SEAIR-made FIB under study, the runway length for takeoff and landing is approximately 200 ft. So, in the world of aviation, especially airplanes, the airfoil concept is needed to improve the optimization of aircraft design.

The advantages of flat plates over airfoils are simplicity of manufacture, cheaper, and easy to repair. If made with the same material, the wing design that uses the airfoil concept will have a higher price because of larger surface area. In addition, the manufacture is also classified as more complicated because it takes more time to determine the curvature of the wings. When viewed from the type of material, the use of composite materials is much better than cloth

(flexible) materials because of their higher hardness properties that can maintain their shape when receiving high air pressure.

In this development, to control the angle of attack of the FIB wing is still manually by moving the frame connected to the wing using both hands. When the pilot is not in a state of alert, at any time the hand can slip from the wing controller unconsciously. So that the wings can experience changes in the angle of attack, both changes in the direction of getting bigger or smaller. A large change in the angle of attack causes a large change in pressure. If the FIB is unable to maintain conditions due to air pressure that is too large, a flip can occur on the FIB. Therefore, the author suggests the existence of a locking system on the FIB wing that can lock the wing position. So that wing control is easier to do, and safety is also increased. This can be done by adding a new section or frame that is able to lock the movement of the frame that controls the movement of the wing. So, when the desired angle of attack has been reached, the frame can be directly placed and locked in the locking system. In addition to the addition of a locking system, the authors suggest the addition of an AOA indicator. The AOA indicator can help provide an indication of the airflow occurring over the wing. AOA indicators provide many benefits for a safe flight (safety flight). By installing this AOA system, we will more easily operate and see the limitations of AOA.

5 CONCLUSION

Based on the simulation that has been carried out on the flat plate flying inflatable boat wing, the lift coefficient increases as the angle of attack increases to an angle of 34° , after passing the 34° angle it decreases. While the drag coefficient continues to increase as the angle of attack increases. At an angle of 34° the lift coefficient has a maximum value, so it is said to be the stall angle, where the stall speed occurs. In this simulation, FIB with flat plate wings has a stall speed of 19.66 m/s (44 mph). Meanwhile, the ratio of lift coefficient to drag coefficient (C_L/C_D) increases as the angle of attack increases to an angle of 5° , after passing through an angle of 5° it decreases. At an angle of 5° the ratio C_L/C_D has a maximum value, so that at this angle we get a cruise speed of 44.7 m/s (100 mph) assuming FIB flies at an altitude of 1,524 m and a cruise speed of 48.28 m/s (108 mph) assuming FIB flies at an altitude of 3,048 m. the greater the ratio C_L/C_D the more aerodynamic the FIB. The effect angle of attack is most significant compare to FIB speed and altitude of the flight.

References

- [1] L. Dawson, 20th Century Passenger Flying Boats, Great Britain, Pen & Sword Aviation, 2021.
- [2] Fédération Aéronautique Internationale, FAI Sporting Code Section 10 Microlight and Paramotor, Switzerland, FAI, 2023.
- [3] A. Pelletier, T. J. Mueller, Low Reynolds Number Aerodynamics of Low-Aspect-Ratio, Thin/Flat/Cambered-Plate Wings. *Journal of Aircraft*, Vol. 37, No. 5, pp. 825 – 832, 2003.
- [4] K. Taira, & T. Colonius, Three-dimensional flows around low-aspect-ratio flat-plate wings at low Reynolds numbers. *Journal of Fluid Mechanics* Vol 623, pp. 187–207, 2009.
- [5] G. E. Torres, & T. J. Mueller, Low Aspect Ratio Aerodynamics at Low Reynolds Numbers. *AIAA Journal*, Vol. 42, No. 5, pp. 865–873. 2004.
- [6] F.M. White, *Fluid Mechanics*, Eighth Edition, McGraw-Hill Education, New York, pp. 462. 2016.

- [7] K. Aldas, & R. Yapici, Investigation of effects of scale and surface roughness on efficiency of water jet pumps using CFD. *Engineering Applications of Computational Fluid Mechanics*, Vol. 8, No. 1, pp. 14–25. 2014.
- [8] L. Casella, W. Langreder, A. Fischer, M. Ehlen, & D. Skoutelakos, Dynamic flow analysis using an OpenFOAM based CFD tool: Validation of turbulence intensity in a testing site, *ITM Web of Conferences*, Vol. 2, pp. 1–12, 2014.
- [9] Federal Aviation Administration, *Airplane flying handbook: Faa-H-8083-3c*, U.S. Department of Transportation, United States, pp. 13, 2021.
- [10] National Aeronautics and Space Administration, *U.S. standard atmosphere*, United States, pp. 52 – 54, 1976.
- [11] Federal Aviation Administration, *Certification of Aircraft and Airmen for the Operation of Light-Sport Aircraft*, U.S. Department of Transportation, United States, pp. 7, 1999.
- [12] M. Shields and K. Mohseni, Effects of Sideslip on the Aerodynamics of Low-Aspect-Ratio, *AIAA Journal*, Vol. 50, pp. 85 - 99, 2012.
- [13] M. A. Lukiantchuki, A. P. Shimomura, F. M. da Silva, & R. M. Caram, Evaluation of CFD simulations with wind tunnel experiments: pressure coefficients at openings in sawtooth building. *Acta Scientiarum. Technology*, Vol. 40, No. 1, e37537, 2018.
- [14] S. B. Punjabi, D. N. Barve, N. K. Joshi, A. K. Das, D. C. Kothari, A. A. Ganguli, S. N. Sahasrabhude, & J. B. Joshi, Computational Fluid Dynamics (CFD) Simulations and Experimental Measurements in an Inductively-Coupled Plasma Generator Operating at Atmospheric Pressure: Performance Analysis and Parametric Study, *Processes*, Vol. 7, No. 3., pp. 133, 2019.
- [15] Q. Wang, Y. Chen, & H. Tang, Mechanism Design for Aircraft Morphing Wing. 53rd AIAA/ASME/ASCE/AHS/ASC Structures, Structural Dynamics and Materials Conference, pp. 1 – 12, 2012.
- [16] S. Jamei, A. Maimun, S. Mansor, N. A. C. Sidik, & A. Priyanto, Design Parametric Study of a Compound Wing-in-Ground Effect. II: Aerodynamics Coefficients, *Journal of Aerospace Engineering*, Vol. 29, No. 1, pp. 1 – 14, 2013.
- [17] Popular Mechanics, The flying boat [online], April 18 2006, availabel: <https://www.popularmechanics.com/adventure/outdoors/a3191/1276901>, (Accessed April 22 2022).